Auxiliary Material: Organic Carbon Burial following the Middle Eocene Climatic Optimum (MECO) in the central - western Tethys

D.J.A. Spofforth[1], C. Agnini[2], H. Pälike[1], D. Rio[2], E. Fornaciari[2], L.

Giusberti[2], V. Luciani[3], L. Lanci[4], G. Muttoni[5]

(1) School of Ocean and Earth Science, University of Southampton, UK

(2) Department of Geosciciences, University of Padua, Italy

(3) Department of Earth Sciences, University of Ferrara, Italy

(4) Instituto Di Dinamica Ambientale, University of Urbino, Italy

(5) Department of Earth Sciences, University of Milano, Italy

———

David JA Spofforth & Heiko Pälike, University of Southampton, School of Ocean and Earth Science, European Way, Southampton, SO14 3ZH, U.K. (david.spofforth@neftex.com, heiko.palike@noc.soton.ac.uk).

1. Age model

A simple age model for the Alano section was initially constructed using linear sedimentation rates between magnetochron boundaries recorded at Alano (figure S1). The astronomically tuned magnetochron ages from *Pälike et al.* [2006a] were used to allow correlation of the Alano record to other globally distributed records from *Bohaty et al.* [2009]. This gave an overall sedimentation rate of 24 m/Myr and constrained the section between 41.05 – 36.5 Ma (41.15 – 36.48 Ma *Cande and Kent* [1995]).

To further constrain the age model two methods were used. Firstly, the δ^{13}C bulk isotope stratigraphy for globally compiled sites [*Bohaty et al.*, 2009] was used to correlate the Alano section within a global isotope stratigraphy, assuming synchroneity between records. In particular the isotopic records from ODP sites 702, 748, 1051 and 1263 were used and 5 correlation tie points (A-E) identified (figure 4 (main text), figure S5). The maximum negative bulk δ^{13}C excursion (B) and following positive excursion (C) were used as primary ties while the 2nd (younger) bulk negative δ^{13}C excursion (D) was used as a secondary tie point along with a pre-main negative excursion point (A) and the decrease following positive δ^{13}C values after the event (E). If the MECO event is assumed to be synchronous then the age model constructed for Alano section suggests that the ~ 100 kyrs older dating for the maximum negative δ^{13}C excursion maybe related to some errors in the construction of the Alano age models or the age models presented in *Bohaty et al.* [2009]. In particular, the magnetochron boundary of C18r / C18n.2n is poorly calibrated at Alano due to problems with running some of the samples. As a result the boundary is placed at 17.22 m above base of section with the last C18r sample at 14.4 m and the

first definitive C18n.2n sample at 19.25 m, with a low positive excursion value at 17.95 m. Within associated errors it is then possible that the correct positioning of the boundary may lie closer to 14.4 m, with the result that the age of the maximum negative bulk $\delta^{13}C$ excursion is younger that the 40.09 Ma calculated using this age model and consistent with the stratigraphic correlation to the records from elsewhere (figure 4, main text) [*Bohaty et al.*, 2009] . We note however, that the apparent synchroneity of the sites in the [*Bohaty et al.*, 2009] records is in part due to isotopic correlation to the records from ODP 702 and IODP site 1051A which have good magnetostratigraphic records and that there maybe some diachroneity between sites.

Difficulties in the placement of the C18n.2r boundary precluded its use within the presented age model. A tentative interpretation places this boundary during the ORG 2 interval where paleodepositional conditions, both during and after deposition, may have affected the signal, while the rapid lithological change may indicate a hiatus during this interval. Nevertheless, if considered, this magnetochron is indicative of a sedimentation rate increase 3 – 6 times the background sedimentation rate during the deposition of ORG2.

Secondly we use biostratigraphic datums to help constrain the position of the MECO event and to positively confirm that the maximum negative δ^{13}C excursion recorded at Alano is the MECO event. Initially in order to better constrain the age model for the Alano section, the geographically close Contessa section [*Lowrie*, 1982; *Jovane et al.*, 2007] (lat. 43º22'47"N; long 13º33'49"E), located in the Umbrian region of Italy, is used to compare magnetostratigraphic ages of key biostratigraphic markers across the MECO event.

The Contessa section provides a high resolution and independent magnetostratigraphy to confirm the ages of events seen at Alano. As the Alano section does not extend as far as the C19n/C18r boundary this also acts to confirm ages at the base of the section where assumptions of constant linear sedimentation may not hold true. However, the Contessa section is affected by low sedimentation rates (5 – 8m/Myrs) and maybe condensed towards the peak of the event. We took magnetochron boundaries from *Jovane et al.* [2007] for C18r and C18n.2n and a simple linear sedimentation rates calculated for each magentochron (Table S1). The dates for the key biostratigraphic datums from both Alano and Contessa, where MECO is recorded, are given in tables S2, S3. From comparison of the Contessa and Alano dating, this appears to again suggest an ∼ 100kyr diachroneity between markers. However, by using purely magnetostratigraphy, rather than astrocyclostratigraphy, we limit the accuracy of placing exact ages on these datums and some diachroneity is likely within the individual species between sites, and Contessa maybe effected by a condensed section towards the top of C18n.2n. In general *Bohaty et al.* [2009] found that the first common occurrence of *Dictyococcites scrippase* marks the beginning of the MECO event, as it does at Alano. Of particular note is the ∼ 100 kyr offset of the species *Orbulinoides beckmanni* and *Sphenolithus furcatolithoides* between Alano and Contessa. As described above, this ∼ 100 kyr older age for MECO, and these datums from a geographically close neighbor, suggests that the positioning of the C18r/C18n.2n. boundary needs to be redefined, but on the basis of matching isotope stratigraphies, and biostratigraphic datums, inparticular *O. beckmanni*, then the maximum negative excur-

sion in δ^{13}C represents the end or the peak of the MECO event as defined by [*Bohaty et al.*, 2009].

2. Geological setting of the Alano di Piave section

The middle/late Eocene Alano di Piave section outcrops in the Belluno Basin in the Southern Alps of NE Italy. This basin formed in the Jurassic as one of four NNE-SSW structural highs and basins (the Friuli Platform, the Belluno Basin, the Trento Platform and the Lombardian Basin) [*Bernoulli and Jenkyns*, 1974; *Bernoulli et al.*, 1979; *Winterer and Bosellini*, 1981] resulting from regional rifting, breaking up and subsequent collapse of Triassic carbonate platforms. Deformation of the African margin (Adria promontory) in the central Tethys seaway and subsequent uplift controlled sedimentation into this area [*Channell*, 1992], evolving from continental margin carbonate shelves in the Triassic [*Channell*, 1992] through to pelagic/hemipelagic settings from lower to upper bathyal environments in the early Cretaceous [*Channell et al.*, 1979; *Channell*, 1992]. Pelagic to hemipelagic lower Paleogene sediments outcrop over a wide area of the basin overlain by turbidite deposits of the Flysch di Belluno from the Friuli Platform to the East to the flanks of the Lessini Shelf to the West where they gradually change into slope facies, mostly hemiplegic pelites [*Zattin et al.*, 2006; *Stefani et al.*, 2007; *Giusberti et al.*, 2007]. The pelagic to hemipelagic sediments of the upper Paleocene to lower Eocene comprise well bedded, pink to red limestone to marly limestones, referred to as the Scaglia Rossa. As clay content increases the Scaglia Rossa grades into the middle Eocene - upper Eocene Marna Scagliosa Cinerea or Scaglia Cinerea (informal formation), which outcrops along the Calcino Creek close to Alano di Piave village (Latitude 45º54'50"N Longitude

11º54'55"E), the focus of this study. This latter formation mainly consists of bathyal grey marls, with occasional indurated limestones beds.

3. Magnetobiostratigraphic methods

These are described in brief below. For a full description please see *Agnini et al.* [(in press) 2010].

3.1. Planktonic Foraminifera and Calcareous Nanofossils

139 samples were prepared using standard methods for analyzes on planktonic foraminifera. Briefly, the indurated marlstones were disaggregated with hydrogen peroxide at concentrations varying from 10 to 30 %. Where needed, samples were additionally treated using Neo-desogen (a surface-tension-active chemical product of the Ciba Geigy Company). Finally, to break up clumps of residue, some samples were placed in a gentle ultrasonic bath. All samples were washed through a 38μm mesh and the finest fraction was separated from the 63μm residue. Biostratigraphic data was obtained using qualitative and quantitative study [*Agnini et al.*, (in press) 2010]. Taxonomic criteria followed are widely explained in *Agnini et al.* [(in press) 2010]. The zonal scheme adopted is that of *Berggren and Pearson* [2005].

Calcareous nannofossils assemblages were studied in 303 samples prepared from unprocessed material following the standard methods of the smear slide and observed in the light microscope at a magnification of 1250x. The average spacing of examined samples is of 60-120 cm, refined to 20 cm immediately across the main biostratigraphic biohorizons. Firstly, all the samples was qualitatively examined and successively analysed with semi-quantitative methods [*Backman and Shackleton*, 1983; *Rio et al.*, 1990] to obtain dis-

tribution patterns of index species. Taxonomy adopted is after *Perch-Nielsen* [1985]. The zonal classification is that of *Martini* [1971].

3.2. Paleomagnetic measurements

Paleomagnetic samples were drilled and oriented in the field at an average sampling interval of 0.6 m giving a total of 159 standard 11 cc specimens for analyses, conducted at the ALP Alpine Laboratory of Paleomagnetism. The intensity of the natural remanent magnetization (NRM), measured on a 2G DC-SQUID cryogenic magnetometer located in a magnetically shielded room, ranges between 0.003 and 8.9 mA/m (mean of 0.270.8 mA/m) with higher values prevalently associated with volcanoclastic-rich intervals. All samples were thermally demagnetized from room temperature to 400–600°C. The component structure of the NRM was monitored after each demagnetization step by means of vector end-point demagnetization diagrams [*Zljderveld*, 1976]. Magnetic components were calculated by standard least-square analysis [*Kirschvink*, 1980] on linear portions of the demagnetization paths and plotted on equal-area projections. Fisher statistics were applied to calculate overall mean directions.

A virtual geomagnetic pole (VGP) was calculated for each characteristic component direction in tilt corrected coordinates. The latitude of the sample characteristic magnetization VGP relative to the mean paleomagnetic (north) pole axis was used for interpreting polarity stratigraphy [*Lowrie and Alvarez*, 1977; *Cande and Kent*, 1995]. VGP relative latitudes approaching +90°N or -90°N are interpreted as recording normal or reverse polarity, respectively. For polarity magnetozone identification, we adopted the nomenclature used by *Cande and Kent* [1995].

4. Inorganic Carbon

4.1. Stable Inorganic Isotopes

Approximately 560 $\delta^{18}O$ and $\delta^{13}C$ isotope measurements from bulk sediment and percentage calcium carbonate ($CaCO_3$) measurements were performed on an EUROPA Scientific GEO 20-20 mass spectrometer fitted with a CAPS CO_3 system. Inhouse standards (Carrara Marble) were measured to evaluate external precision. Results are reported relative to the Vienna Pee Dee Belemnite (VPDB) standard with an external analytical precision (1σ), based on replicate analysis of an inhouse standard calibrated to NBS-19 of 0.028‰ for $\delta^{13}C$ and 0.057‰ for $\delta^{18}O$. Where necessary, additional samples were prepared and repeated to check for homogeneity within the sediment. These gave a repeatability (1σ) of 0.037‰ for $\delta^{13}C$ and 0.081‰ for $\delta^{18}O$.

4.2. CaCO₃ content

Elemental composition for $CaCO_3$ was calculated using linear extrapolation based on the beam height response to the amount of carbonate present in the sample measured on the EUROPA Scientific GEO 20-20 isotope mass spectrometer. Over 100 standards of different masses between $\sim$ 200 - 480 μg were used to produce a linear best fit line (figure S6) with R^2 = 0.94 - 0.99 (see supplementary information). Results were validated using a H-C-N-O elemental analyzer (figure S7).

5. Organic Carbon measurements

5.1. Preparation of TOC material

Samples were dried, crush and ground to a homogenous fine powder using either agate pestle and mortar or a agate grinding mill. $\sim 2 - 3$ g of material were then placed in test

tubes and 37% HCl added drop wise until all the material had reacted. $\sim 3 - 4$ ml of HCl were added and the samples left overnight. The samples were then neutralized using milli-Q water through a repeated process of siphoning off liquid, mixing with milli-Q and settling. Once neutralized, samples were pipetted into vials and placed in an oven at 50°C. Dried residues were ground, dried and stored. $\sim$ 3mg of both decalcified sample and $\sim$ 3mg of original sample material were weighed in to tin foil cups and measured for total Organic Carbon (TOC) using an H-C-N-O elemental analyser. A certified standard containing 6.1% C was used. Sample standard deviation was 0.065 % based on 10 standard samples. TOC was calculated using the equation

$$TOC\% = 100 \times (\frac{8.33 \times TC}{100 - 1}) \div (\frac{8.3 - 100}{AC}) \qquad (1)$$

CaCO$_3$ was calculated using the same samples were used as for TOC however equation (2) was applied.

$$\%CaCO_3 = 100 \times (1 - TOC/AC) \qquad (2)$$

5.2. Preparation of organic residues

In brief, samples were broken into $\sim$1mm^2 pieces and placed in 250 ml beakers and 37% HCl was added dropwise until no further reaction. Then $\sim$ 1cm^3 of HCl was added and left overnight. Samples were then neutralized using water and after settling the excess liquid decanted. Subsequently $\sim$ 60% HF was added dropwise until visible reaction had finished and $\sim$ 200ml of HF added and left to react overnight. Samples were again neutralized and the excess liquid decanted. Samples were then filtered through a 10μ sieve and the

residue collected and boiled with 37% HCl for 1 minute before been filtered again to remove possible CaF crystals. Once the residue has settled the excess liquid was decanted and the sample transferred to a vial via a third sieving process.

Glass slides were prepared for each sample to allow identification of organic material.

5.3. TOC measurements

TOC measurements were made on 3 mg of both decalcified sample and $\sim$ 3mg of original sample material were prepared following standard procedures, weighed into tin foil cups and measured for total organic carbon (TOC) using an H-C-N-O elemental analyser. A certified standard (high organic content sediment standard) containing 6.1% C was used. Sample standard deviation was 0.065 % based on $\geq$10 standard samples.

Organic material was then extracted from 10 samples over the investigated interval ranging from 0.1 - 3% TOC using the method described in [*Morgans-Bell et al.*, 2001]. Non-oxidising acids HCl and HF were used to demineralise the samples. An oxidation step to remove pyrite and other sulphur based heavy minerals was not used as this would alter the organic material. Glass slides were then prepared for the identification of organic material.

5.4. Organic Carbon isotopes

Measurements of $\delta^{13}C$ of organic material were performed using decarbonated samples on an Euro Elemental Analyser (EA). Samples were decarbonated using the same procedure as for TOC analysis (supplementary informaion), dried and then weighed into isotope grade tin cups. For all samples, a targeted beam height of 4nA was used and the mass of sample required was calculated using the results from TOC measurements. A

low organic soil certified reference containing 1.6% organic carbon was used as a standard with an external analytical precision (1σ), based on replicate analysis of this standard of 0.045‰ for δ^{13}C. Where necessary, additional samples were prepared and repeated to check for homogeneity within the sediment. These gave a repeatability (1σ) of 0.096‰ for δ^{13}C.

6. Sediment Geochemistry

Samples were analyzed using quantitative XRF over the interval from $\sim$ 13m - 30m in order to characterize changes in paleo-environment during the MECO event identified from the isotope record. In brief, samples were dried, ground and homogenized (agate ball mill), dried and then $\sim$ 3mg of powder were pressed into a pellet for analysis. These were analyzed for major and minor elements using a Phillips PW1400 X-ray spectrometer and analytical precision based on repeated reference material and sampled ranged from $\sim$ 0.1– 5% (Table S1). For reconstructing paleoenvironmental conditions using trace elements the relative enrichment or depletion of the sediment with respect to each trace element is required. Any $CaCO_3$ present dilutes the trace element abundance signal and increased detrital material will increase the absolute concentrations of individual samples therefore all trace elements are normalised to Al [*Wedepohl*, 1971; *Calvert and Pedersen*, 1993; *Van der Weijden*, 2002].

7. Determining $CaCO_3$ content of samples

The principal data set of $CaCO_3$ content in the Alano di Piave samples was acquired using calibration of the ion beam heights on the mass spectrometer. As this technique

had not previously been applied to the EUROPA Scientific GEO 20-20 isotope mass spectrometer before at the National Oceanography Centre, Southampton it was necessary to validate this method. Two different techniques were used for this: 1) Coulometry and 2) H-C-N-O Elemental analysis. This section briefly describes the methods used and presents statistical results showing that the results produced from the mass spectrometer (GEO) are robust.

The principal aim of developing the mass spectrometry $CaCO_3$ method was that it would simultaneously produce a % $CaCO_3$ record at the same time as the stable isotope record. The most important aim was that relative changes in $CaCO_3$ content through the section would be recorded accurately for potential use in orbital analysis and sedimentation rate studies and secondly ideally the values produced would be correct.

Elemental composition for $CaCO_3$ was calculated using linear extrapolation based on the beam height response to the amount of carbonate present in the sample measured on the EUROPA Scientific GEO 20-20 isotope mass spectrometer. The $CaCO_3$ in a sample when dissolved produces CO_2 gas. The pressure of this CO_2 gas when squeezed up in the bellows is measured and generates a current, the beam height. The pressure of CO_2 gas is directly proportional to the beam height and therefore the mass of carbonate in the sample.

7.1. $CaCO_3$ determined using beam height calibration

In each machine run 5 individually weighed SC1 standards were measured and then graphically plotted to form a best fit linear calibration of beam height to mass of $CaCO_3$ in the sample. The standard, SC1, was assumed to be 100% $CaCO_3$ and this was verified

using the coulometer with a mean value of 100.1 % CaCO$_3$ (1σ=0.46). Standards and samples were weighed such they had an estimated CaCO$_3$ content of $\sim$ 200 - 480 μg to ensure they would fall in the unbalanced bellows in the mass spectrometer. If CO$_3^{2-}$ content, by mass, was below this the sample was transferred to the cold finger, while values above are placed into the balanced bellows. This allowed isotope data to still be obtained and a working estimate of CaCO$_3$ to be made for re-analysis.

Typical least squares regressions linear fits of the data produced correlation coefficients (R^2) > 0.95. Data from multiple mass spec runs could then be added together to produce a more robust best fit line with a large number of data points (> 75) (figure S6). The high level of repeatability of the results suggests that the machine linearity is stable and that likely small errors associated with weighing of samples ($\sim \pm 0.03$ μg), sample loss on transfer, and incomplete squeezing up of the bellows are either small or constant. However, through time changes in the sensitivity of the mass spectrometer to the amount of CaCO$_3$ do occur and are illustrated by the two separate best fit lines in figure S6 representing a series of runs several months apart (November and February).

7.2. % CaCO$_3$ determination using the coulometer

In order to determine the approximate CaCO$_3$ of the samples before running on the mass spectrometer a study of 52 samples at $\sim$ 0.6 metre spacing between 42.83 m and 74.01m from the Alano di Piave section were measured for CaCO$_3$ content by coulometric titration with a UIC model 5012 CO$_2$ coulometer. Samples of approximately 100 mg were taken from gross samples and placed in an oven at $\sim$ 60°C to dry for approximately 48 hrs. Samples were then ground to powder in an agate mortar (this is primarily used to

prevent metal contamination if remaining sample is needed for trace metal analysis at a later stage.) From these $\sim$ 25 mg samples were weighed out and this weight noted (The remainder of the bulk sample was kept for repeats or for the stable isotope analysis or trace metals.) In order to determine the percentage content of $CaCO_3$ the CO_2 concentration liberated by 10% phosphoric acid on the sample is measured. Calibration of the instrument was performed using a pure $CaCO_3$ standard. Reference standard sediment 105491K (pure $CaCO_3$) was run at the beginning, middle and end of the measurements to check the calibration of the instrument, followed by a blank. One sample was repeated to double check the measurements. Replicates based on the $CaCO_3$ standard and the GEO SC1 standard gave 1σ values of 0.36 and 0.46 respectively. Figure S7 shows the coulometer data (black) plotted against the GEO data (blue) for this interval.

7.3. % CaCO$_3$ determination using the Elemental analyser

Percentage $CaCO_3$ was calculated using a H-C-N-O elemental analyser (EA) on the same bulk samples as used for total organic carbon (TOC) measurements (see preparation description below) and the following equation (Eq 3) was applied. Figure S8 shows the EA data (red) plotted against the GEO data (black) for this interval.

$$\%CaCO_3 = 100 \times (1 - TOC/AC) \tag{3}$$

where AC is the non-decarbonated sample and TOC is the total organic carbon content of the sample calculating using EQ 1

8. Statistical comparison of estimation methods

Both the coulometer and EA techniques when compared to the results from the GEO produce similar mean values within an error of 1 standard deviation (Tables S4, S5) suggesting that the values recorded by the GEO are correct. Visually both techniques appear have be a strong positive correlation between the shape of each data set (figures S8, S7). Although, both visually and from the close agreement of the mean values the data appear to be drawn from the same population it is necessary to test this assumption if the $CaCO_3$ record from the mass spectrometer is to be considered reliable. Each individual depth measurement was carried out using two methods we assume that each $CaCO_3$ value is paired (as acquired from same hand sample) and as such the null hypothesis is that the data are taken from the same population. The Kolmogorov-Smirnov test is used to determine if this is the case. For each data set the normalised cumulative distribution (using the total % $CaCO_3$ over the selected interval) is calculated (figure S9), and then the difference in values between the two curves at each corresponding depth point is calculated. This value (D) is plotted in figure S10 falling within the acceptance of the null hypothesis for both depth intervals measured. The Kolmogorov-Smirnov test is particular appropriate as it does not assume any knowledge of the population from which the samples were drawn.

Although the Kolmogorov-Smirnov test shows that the data sets are from the same population it is also necessary to calculate a measure of how well the two records correlate to each other. If we assume that the data do represent a normal gaussian distribution, then at depth each point has two individual readings these can be seen as paired points, I.e. the

lowest value should correspond to the lowest value etc... Therefore a simple least squares linear regression should give a measure of how well the two data sets correlate. R^2 values of 0.58 and 0.76 are found for the coulometer and EA comparison respectively. However, the calculated regression is strongly affected by the effect of outliers, for example, the points at 69.41 m (figure S8) in the coulometer readings and a more robust fit is required. Two better statistical tests of the correlation are the Pearson product-moment correlation coefficient and the Spearman's rank correlation coefficient (Tables S4, S5). These both strongly indicate that there is a strong correlation between the individual data sets over the selected intervals with a 95% confidence interval for the latter test. The Spearman test is applicable to this data set as it ranks the data from each method from lowest to highest and each value is given a score (1, 2, 3, and so on). Therefore the lowest value in one data set should correspond to the lowest value in the other data set, this allows outlying values to be considered.

Based on the results of these individual statistical tests the estimation of $CaCO_3$ using beam height calibration of the mass spectrometer is a robust method and can be considered reliable.

References

Agnini, C., et al. ((in press) 2010), Integrated Bio-magnetostratigaphy of the Alano di Piave section (NE Italy): A proposal and definition

of the middle–late Eocene boundary, *GSA Bulletin*.

Backman, J., and N. J. Shackleton (1983), Quantitative biochronology of Pliocene and early Pleistocene calcareous nannofossils from the

Atlantic, Indian and Pacific oceans., *Marine Micropaleontology*, *8* (2), 141–170.

Berggren, W. A., and P. N. Pearson (2005), A revised tropical to subtropical paleogene planktonic foraminiferal zonation, *Journal of*

Foraminiferal Research, *35* (4), 279–298.

Bernoulli, D., and H. C. Jenkyns (1974), Alpine, Mediterranean and Central Atlantic Mesozoic Facies in relation to the early evolution

of the Tethys, in *Modern and Ancient Geosynclinal Sedimentation, Special Publication*, vol. 19,

edited by J. Dott, R. H. and R. H. Shaver, pp. 19–160, Society for Sedimentary Geology (SEPM).

Bernoulli, D., C. Caron, P. Homweood, O. Kalin, and J. Van Stuijvernberg (1979), Evolution of continental margins in the Alps, *Schweiz-*

erische Mineralogische und Petrographic Mitteilungen, *59*, 165–170.

Bohaty, S. M., J. C. Zachos, F. Florindo, and M. L. Delaney (2009), Coupled greenhouse warming and deep-sea acidification in the middle

Eocene, *Paleoceanography*, *24*, doi:10.1029/2008PA001676.

Calvert, S. E., and T. F. Pedersen (1993), Geochemistry of Recent Oxic and Anoxic Marine-Sediments - Implications for the Geological

Record, *Marine Geology*, *113* (1-2), 67–88.

Cande, S. C., and D. V. Kent (1995), Revised Calibration of the Geomagnetic Polarity Timescale for the Late Cretaceous and Cenozoic,

Journal of Geophysical Research-Solid Earth, *100* (B4), 6093–6095.

Channell, J. E. T. (1992), Paleomagnetic data from Umbria (Italy) - Implications for the rotation of Adria and Meozoic apparent polar

wander paths., *Tectonophysics*, *216* (3-4), 365–378.

Channell, J. E. T., B. Dargenio, and F. Horvath (1979), Adria, the african promontory, in mesozoic mediterranean paleogeography, *Earth-*

Science Reviews, *15* (3), 213–292.

Giusberti, L., D. Rio, C. Agnini, J. Backman, E. Fornaciari, F. Tateo, and M. Oddone (2007), Mode and tempo of the Paleocene-Eocene thermal maximum in an expanded section from the Venetian pre-Alps, *Geological Society of America Bulletin*, *119*, 391–412.

Jovane, L., F. Florindo, R. Coccioni, J. Dinarès-Turell, A. Marsili, S. Monechi, A. P. Roberts, and M. Sprovieri (2007), The middle Eocene climatic optimum event in the Contessa Highway section, Umbrian Apennines, Italy, *Geological Society of America Bulletin*, *119*(3), 413–427.

Kirschvink, J. L. (1980), The least-squares line and plane and the analysis of paleomagnetic data, *Geophysical Journal of the Royal Astronomical Society*, *62*(3), 699–718.

Lowrie, W. (1982), A revised magnetic polarity timescale for the cretaceous and Cainozoic, *Philosophical Transactions of the Royal Society of London Series A-Mathematical Physical and Engineering Sciences*, *306*(1492), 129–136.

Lowrie, W., and W. Alvarez (1977), Late Cretaceous geomagnetic polarity sequence - detailed rock and paleomagnetic studies of Scaglia Rossa limestone at Gubbio, Italy, *Geophysical Journal of the Royal Astronomical Society*, *51*(3), 561–581.

Martini, E. (1971), Standard Tertiary and Quaternary calcareous nannoplankton zonation, in *2nd Planktonic Conference*, vol. 2, edited by A. Farinacci, pp. 739–785, Tecnoscienza, Roma.

Morgans-Bell, H. S., A. L. Coe, S. P. Hesselbo, H. C. Jenkyns, G. P. Weedon, J. E. A. Marshall, R. V. Tyson, and C. J. Williams (2001), Integrated stratigraphy of the Kimmeridge Clay Formation (Upper Jurassic) based on exposures and boreholes in south Dorset, UK, *Geological Magazine*, *138*(5), 511–539.

Pälike, H., R. D. Norris, J. O. Herrle, P. A. Wilson, H. K. Coxall, C. H. Lear, N. J. Shackleton, A. K. Tripati, and B. S. Wade (2006a), The Heartbeat of the Oligocene Climate System, *Science*, *314*(5807), 1894–1898, doi:10.1126/science.1133822.

Perch-Nielsen, K. V. (1985), Cenozoic calcareous nannofossils, in *Plankton Stratigraphy*, edited by H. M. Bollis, pp. 427–554, Cambridge University Press.

Rio, D., I. Raffi, and G. Villa (1990), Pliocene–Pleistocene calcareous nannofossil distribution patterns in the western Mediterranean, in *Proc. Ocean Drill. Program Sci. Results*, vol. 107, pp. 513–533.

Stefani, C., M. G. Fellin, M. Zattin, G. G. Zuffa, C. Dalmonte, N. Mancin, and A. Zanferrari (2007), Provenance and paleogeographic evolution in a multi-source foreland: The Cenozoic Venetian-Friulian Basin (NE Italy), *Journal of Sedimentary Research*, *77*(11-12), 867–887, doi:DOI10.2110/jsr.2007.083.

Van der Weijden, C. H. (2002), Pitfalls of normalization of marine geochemical data using a common divisor, *Marine Geoloy*, *184*(3-4), 167–187, doi:10.1016/S0025-3227(01)00297-3.

Wedepohl, K. H. (1971), Environmental influences on the chemical composition of shales and clays, in *Physics and Chemistry of the Earth*, vol. 8, edited by L. Ahrens, F. Press, S. Runcorn, and H. Urey, pp. 305–333, Pergamon, Oxford.

Winterer, E. L., and A. Bosellini (1981), Subsidence and sedimentation on Jurassic passive continental-margin, Southern Alps, Italy, *Aapg Bulletin-American Association of Petroleum Geologists*, *65*(3), 394–421.

Zattin, M., A. Cuman, R. Fantoni, S. Martin, P. Scotti, and C. Stefani (2006), From Middle Jurassic heating to Neogene cooling: The thermochronological evolution of the southern Alps, *Tectonophysics*, *414*(1-4), 191–202, doi:DOI10.1016/j.tecto.2005.10.020.

Zljderveld, J. A. (1976), Comparative thermal and alternating magnetic-field demagnetizations, in *Transactions-American Geophysical Union*, vol. 57, pp. 653–653, AGU, Washington, DC.

Table S1.   Position of magnetochron boundaries for the Contessa section taken from *Jovane et al.* [2007] used to calculate age of key biostraigraphic datums, *O. beckmanni, S.furcatolithoidies*

Magnetochron	Top depth	Base Depth	LSR (m/Myr)
C18r	135.29	128.63	5.26
C18n.2n	139.21	135.28	8.13

Table S2.   Position of key biostratigraphic datums for the Contessa section taken from *Jovane et al.* [2007] for comparison to the Alano Di Piave section

Occurence	Datum	Datum pos. (m)	Age (Ma)
FCO	*D. scripase*	137	39.87
LO	*O.beckmanni*	137	39.87
FO	*O.beckmanni*	135	40.14
LO	*S.furcatolithoidies*	132.6	40.6

Table S3.   Position of key biostratigraphic datums for the Alano di Piave section

[*Agnini et al.*, (in press) 2010]

Occurence	Datum	Datum pos. (m)	Age (Ma)
LO	*O.beckmanni*	19.5	39.95
FO	*O.beckmanni*	14.4	40.24
LCO	*D.bisectus*	9.5	40.52
FCO	*D. scripase*	9.3	40.54
LO	*S.furcatolithoidies*	6.3	40.707

Table S4.   Statistical analysis of the correlation between % $CaCO_3$ estimation using

the Coulometer and mass spectrometer over Alano interval 47 - 73m. Total number of

samples is 104. Pearson coefficient and Spearman rankings are correlations where a value

of 1 is perfect correlation (CF is the correlation factor).

	Geo	Coulometer	CF
Mean	45.06	46.85	
σ	3.45	4.92	
Least squares(R^2)			0.59
Pearson coefficient			0.76
Spearman ranking			0.64

Table S5.   Statistical Analysis of the correlation between % CaCO$_3$ estimation using the elemental analyser (EA) and mass spectometer (GEO) over Alano interval 10 - 30m. Pearson coefficient and Spearman rankings are correlations where a value of 1 is perfect correlation. (CF is the correlation factor)

	Geo	EA	CF
Mean	41.2	42.4	
σ	7.85	8.11	
Least squares (R^2)			0.76
Pearson coefficient			0.87
Spearman ranking			0.94
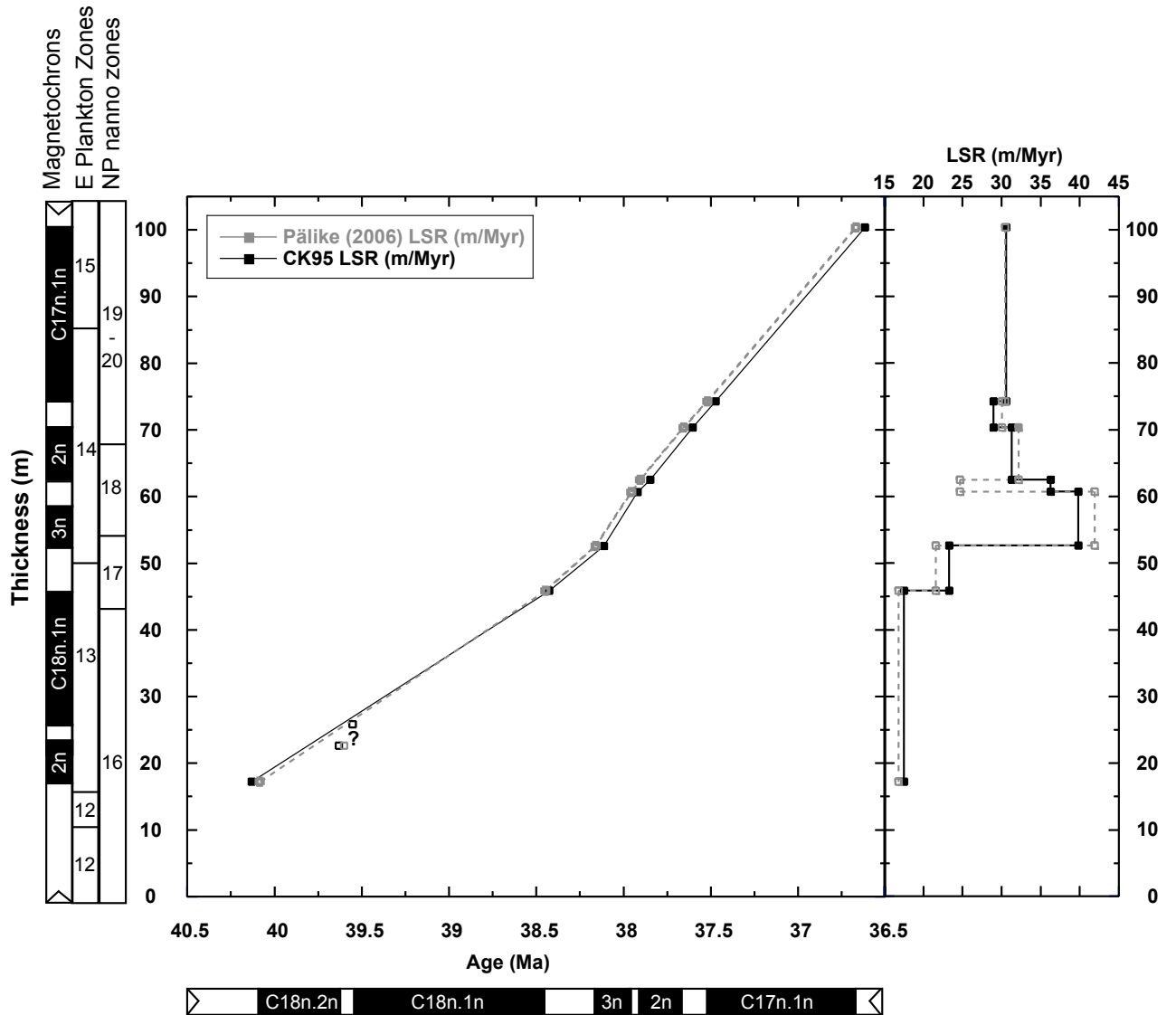
Figure S1. Age Model construction for the Alano section using magnetostratigraphy. Ages are taken from [Cande and Kent 1995] and [Palike et al. 2006]. Sedimentation rates are constructed assuming linear sedimentation between tie points.
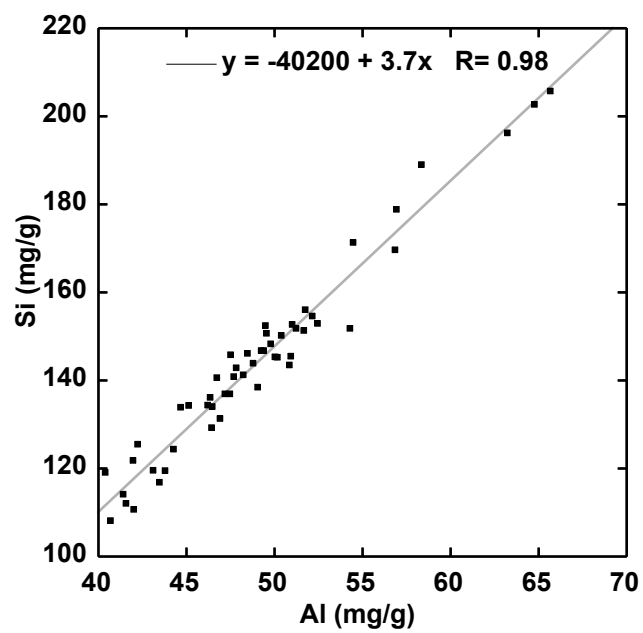
Figure S2. Al concentration vs. Si scatterplot.
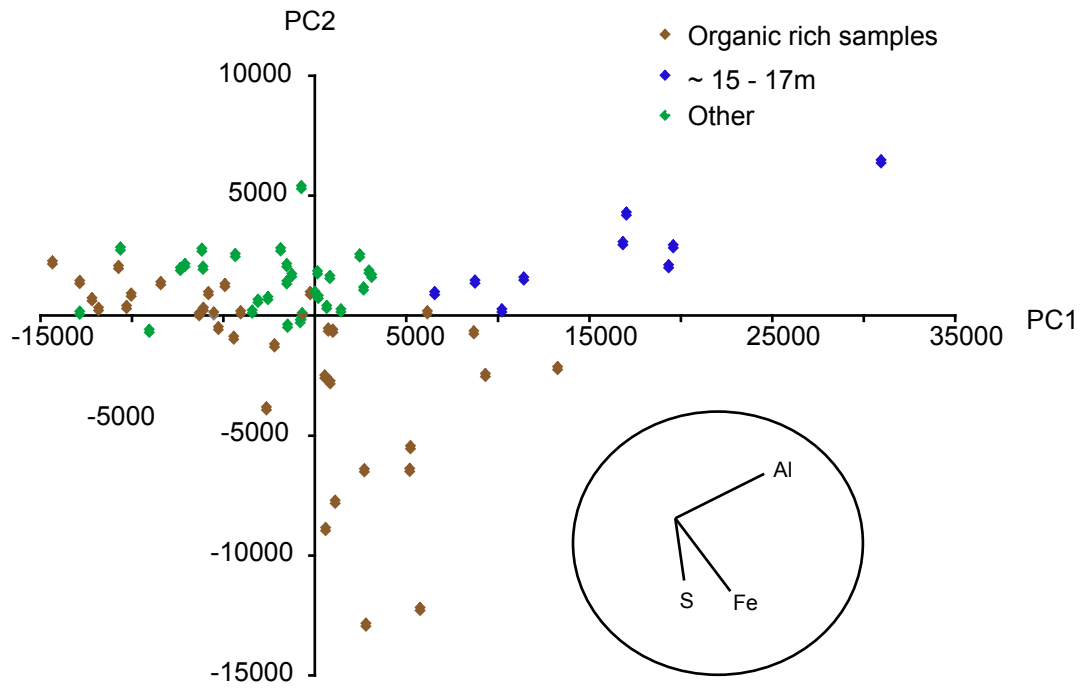
Figure S3.   Principal Component Analysis of geochemical data over the MECO interval. The eigenvector directions of Al, Fe and S are shown in the bottom right of the figure. Discrete samples are labelled as in key. PC1 represents Al and PC2 is Fe.
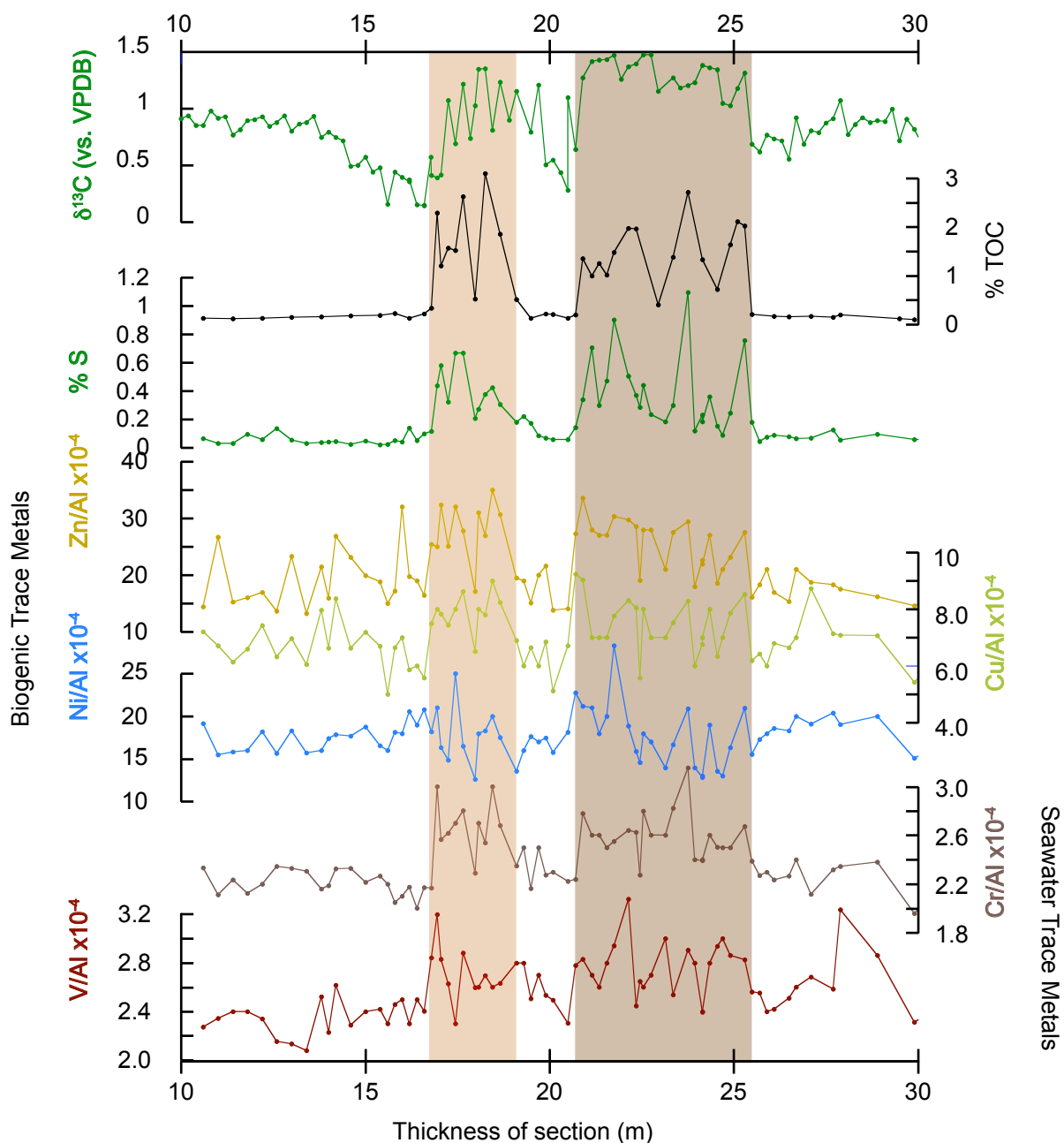
Figure S4.   Sediment Geochemistry across the MECO interval. From top $\delta^{13}C_{cc}$ and $\delta^{13}C_{org}$, %

sulfur, Zn/Al, Cu/Al, Ni/Al, Cr/Al, V/Al. Elemental data measured on discrete XRF samples.

Overlaid bands indicate organic rich intervals.
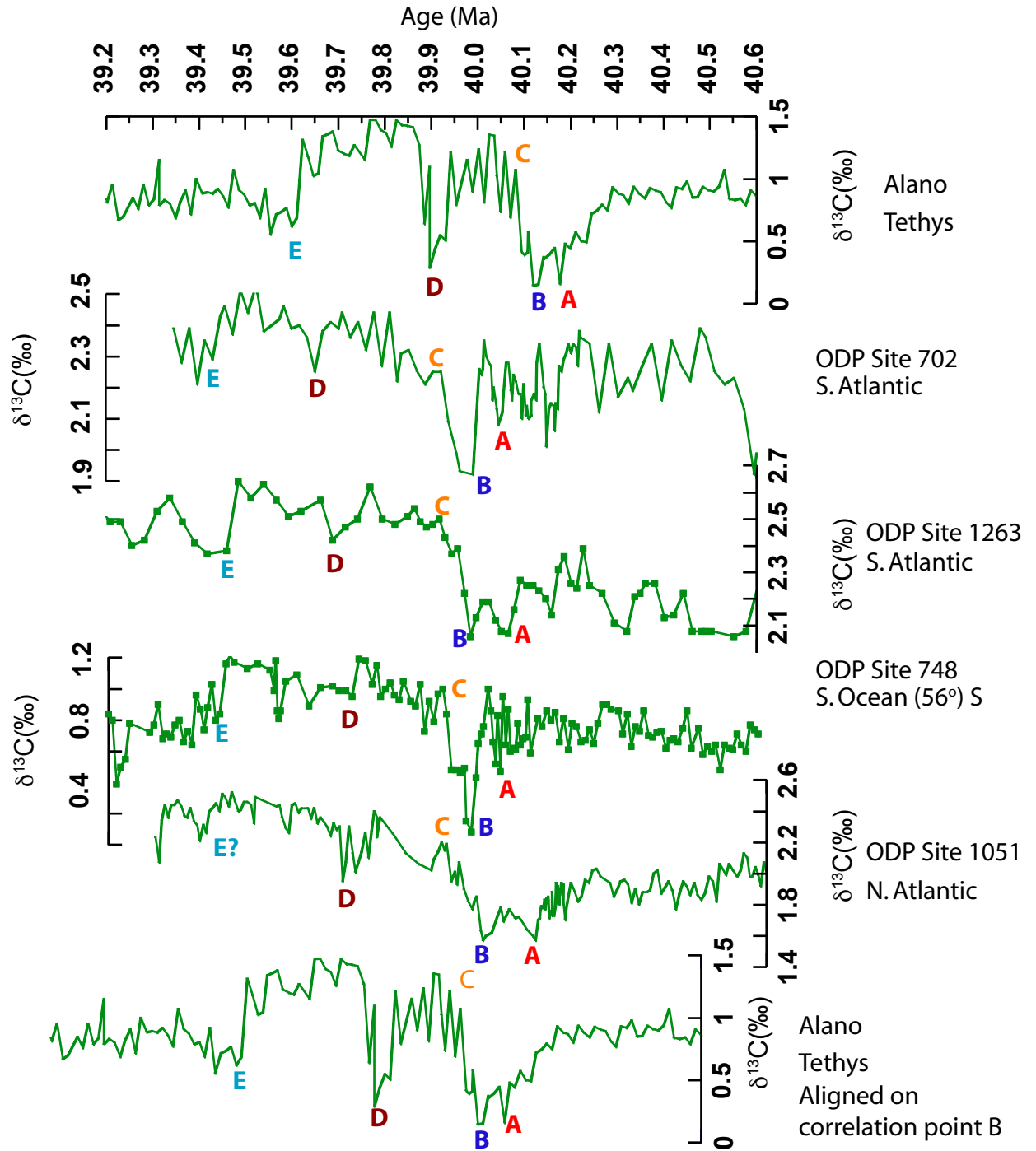
Figure S5. Tie points for δ^{13}C stratigraphy for the Alano to section to previous records [*Bohaty et al.*, 2009]. 5 possible tie points are identified and labeled A to E. The bottom record shows the Alano record aligned on point B.
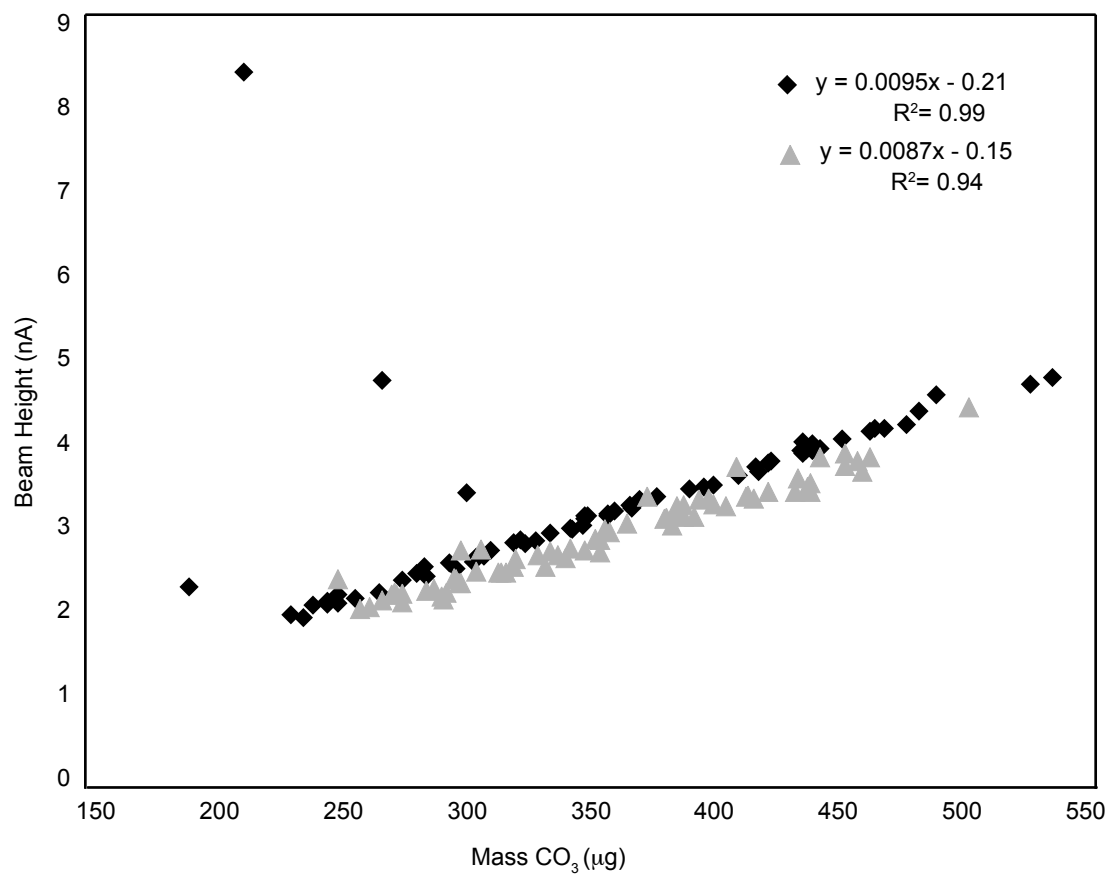
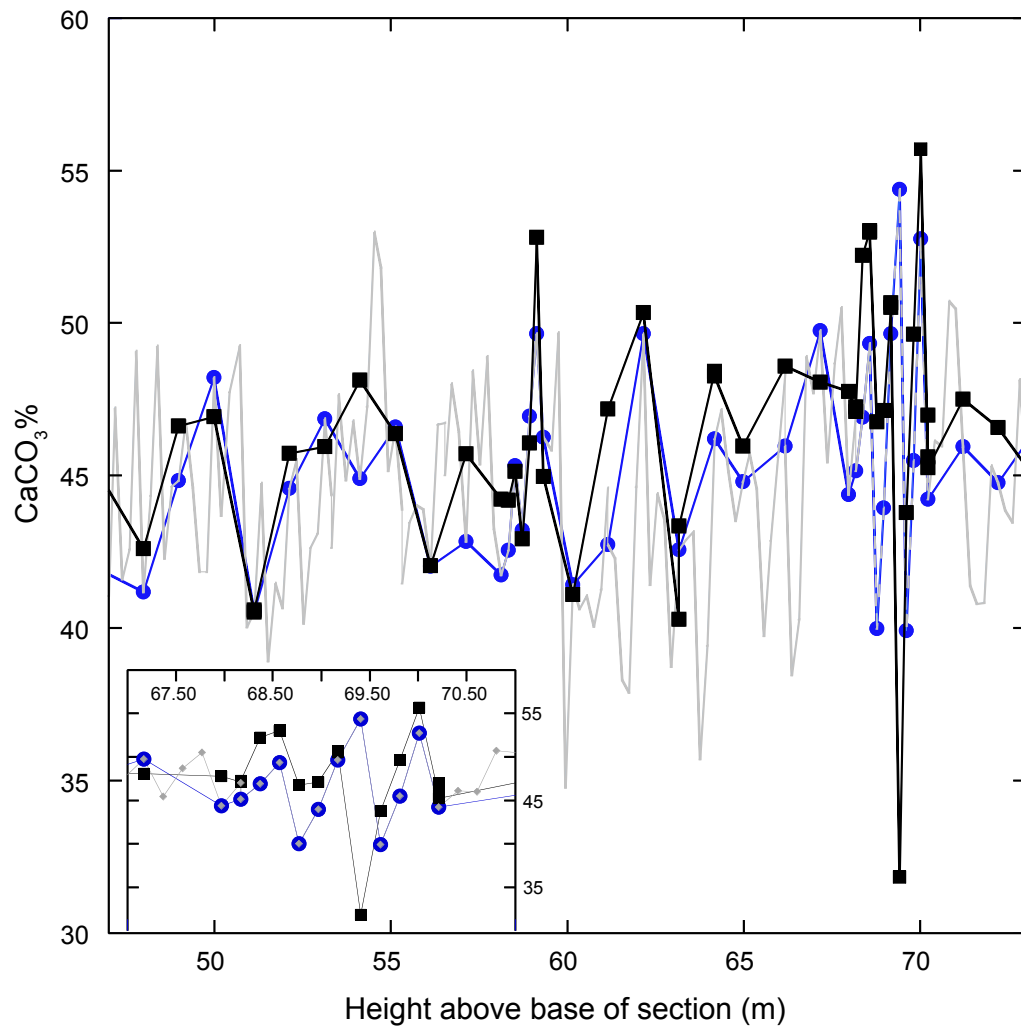**Figure S6.**   Calibration line for CaCO$_3$ calculated from the Europa Scientific GEO 20-20 mass spectrometer.

Figure S7. % CaCO₃ records over the interval 43 - 74 m above base of section from the Alano Di Piave outcrop (chapter 4). % CaCO₃ records calculated using beam height calibration (black) and a coulometer (blue) are shown. The light grey record is the complete CaCO₃ record calculated using the mass spectrometer. The inset shows the interval from 67.25 - 70.75 m above base of section in more detail.
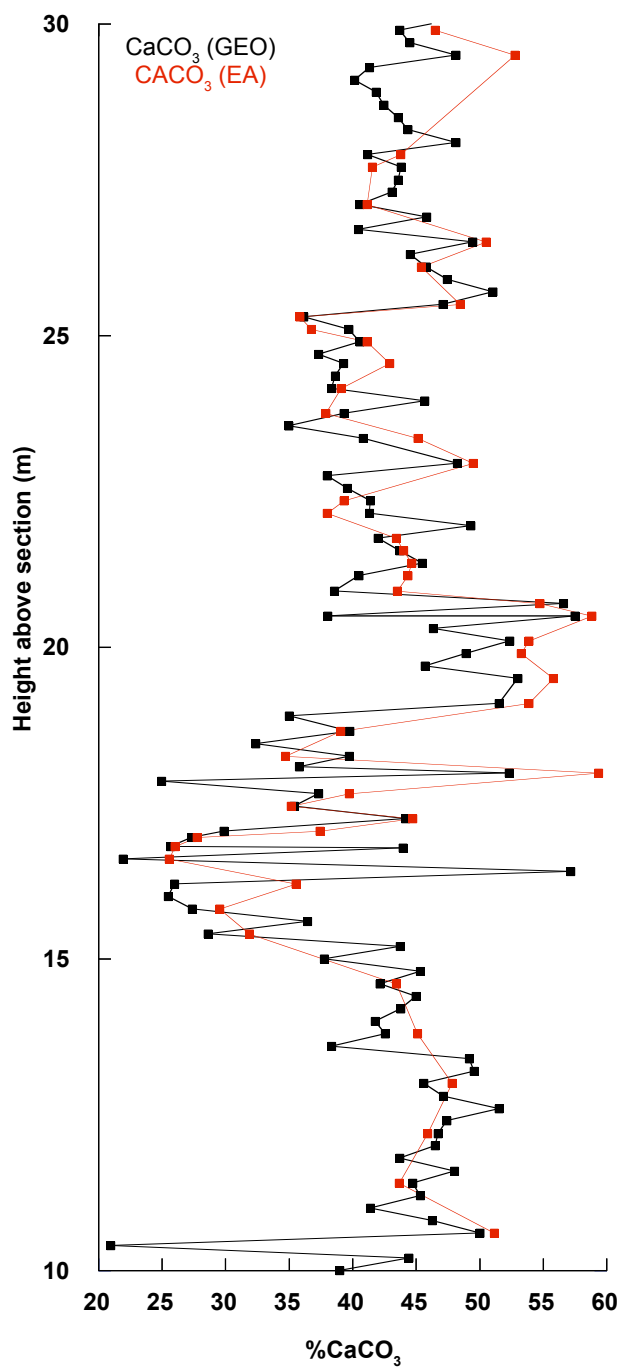
Figure S8. Comparison of calculation methods for CaCO₃ using the calibration of beam heights from the figure S1 and measured using an elemental analyser.
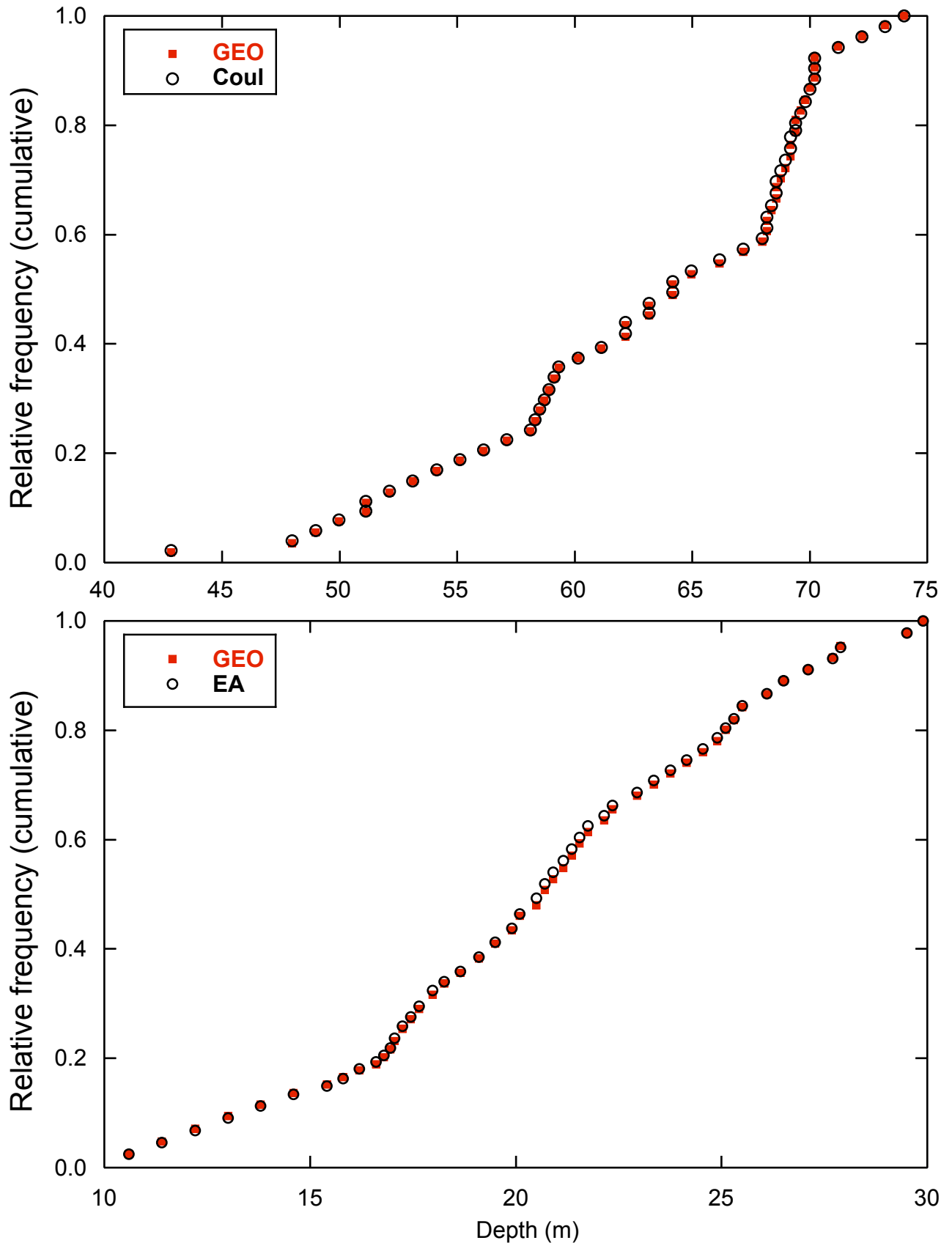
Figure S9.   Normalised cumulative frequency plots versus height above base section for the
Alano Di Piave section for the comparison intervals 43-74 m (top) and 10 - 30m (bottom). GEO

data in red and either coulometer or elemental analyser in black (see legend). For description of
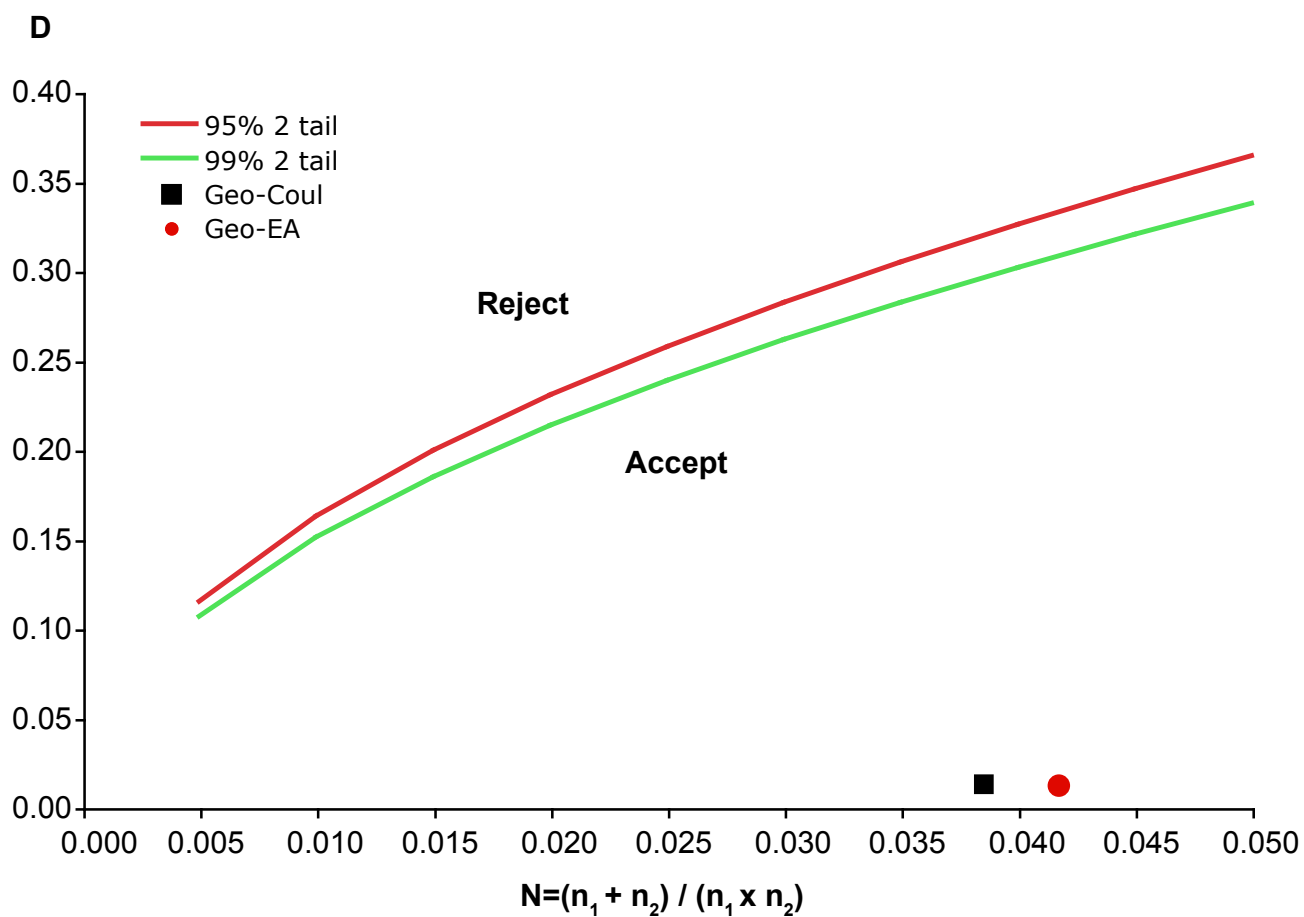
method see main text.

Figure S10. Kolmogorov-Smirnov test plot. The difference (D) between cumulative frequency curves is plotted against a function of sample sizes. Acceptance limits are plotted at 95% and 99% confidence intervals.